Improvement of Ride Comfort Quality for an Earth-Moving machinery with Semi-Active Cab Isolation System

Le Van Quynh[1*], *Dang Viet* Ha[2], *Bui Van* Cuong[1], *Le Anh* Vu[3], and *Tran Van* Thoan[3]

[1]Faculty of Automotive and Power Machinery Engineering, Thai Nguyen University of Technology, Thai Nguyen, Vietnam
[2]Vietnam Register, Ha Noi 12059, Viet Nam
[3]Faculty of Automobile Engineering, Hung Yen University of Technology and Education, Hung Yen, Viet Nam

Abstract. Improving ride comfort of earth-moving machinery is important to avoid potential health hazards for machine operator. A vehicle - road coupled interaction model including vehicle body, cab body and driver seat masses is set up under the random excitation of ground surface and a Fuzzy –PID controller is designed for control of the damping coefficient of a semi-active hydraulic cab isolation system (SHCIs) for an earth-moving machinery. The ride performance of SHCIs with a combined controller is evaluated under different movement conditions. The comparison results indicate that the proposed controller for semi-active cab hydraulic isolation system has the significantly improved vehicle ride comfort in compared with passive hydraulic cab isolation system (PHCIs) under large amplitude and low frequency excitations of ground surface.

1 Introduction

Earth-moving machinery usually operates in harsh working conditions such as off-road, noise and changing load conditions. On the other hand, vehicles are often not equipped with the suspension to link between the axles and vehicle body. Vibration sources are transmitted to driver body via cab isolation system and seat suspension system. In order to reduce the adverse effects caused by vibrations on the operator and vehicle durability, the researchers are constantly looking for ways to improve the design of the vehicle cab and driver seat suspension system. To evaluate the effect of an earth-moving machinery vibration on vehicle ride comfort and health performance of humans, the experiments were conducted and measured the vibrations transmitted to the whole body (WBV: whole-body vibration) according to ISO 2631-1 and 2631-5 standards with measurement results across three different front-end loader tire configurations [1], both two standards, ISO 2631-1(1985) and ISO 2631-1 (1997) with measurement results in the 11 operations [2], both two standards, ISO 2631-1(1997) and ISO 2631-1(2004) with different operations [3], and the order tracking technique (OTT) and transmission path analysis (TPA) with measurement results under the vibration sources of the earth-moving machinery [4]. The dynamic models of the earth-moving machinery with 3 DOF were proposed to analyze vehicle ride comfort with or without vibration absorber system [5]. A multibody dynamic model of earth-moving machinery with 5 DOF was proposed to analyze the vehicle ride comfort and the simulation results were verified by the experimental results ride comfort [6]. A multibody model of earth-moving machinery was proposed to evaluate the ride performance of the suspended wheel axles in comparing with unsuspended axles [7]. In order to improve vehicle ride comfort, the hydro-pneumatic suspension of earth-moving machinery was proposed to analyze the effects of it on the vehicle ride comfort, driving stability and operational stability based on a multibody model using RecurDyn in co-simulation with MATLAB/Simulink [8]. The optimal parameters of the hydro-pneumatic suspension of earth-moving machinery were found out and then, a fuzzy controller was designed to realize the active adjustment of the suspension parameters under the different operating conditions [9]. A hybrid model predictive control (HMPC) strategy is proposed to control the on-off statuses of switch electromagnetic valves of the shock absorber of semi-active axle suspension system of earth-moving machinery based on the hybrid dynamical model [10].

The limited construction machine suspension system easily causes motion instability during machine operation. Therefore, cab's isolation systems are important to reduce the vibration sources transmitted to the operator's body. The hydraulic mounts were proposed to evaluate the effects of its characteristics on vehicle ride comfort based on a 6-DOF dynamic model of cab [13]. Three different cab's isolation mounts were respectively surveyed and analyzed their effects on vehicle ride comfort based on a 3-D nonlinear dynamic model [14]. The optimal parameters of cab isolation system were found by the multi-objective genetic algorithm (MOGA) [15], a unique computer aided engineering

*Corresponding author: lequynh@tnut.edu.vn

(CAE) method [16, 20], and the genetic algorithm (GA) [17, 18]. A combined control method of Fuzzy and PID control was proposed to control the damping coefficient of semi-active cab isolation system of soil a single drum vibratory roller based on a non-linear vehicle dynamic model [19].
The main aim of this study is to control the value of damping coefficient for a semi-active hydraulic cab isolation system (SHCIs) for enhancing the ride comfort of a wheel loader. A vehicle - road coupled interaction model of a wheel loader is set up under the random excitation of ground surface and a Fuzzy –PID controller is designed for control of the damping coefficient of (SHCIs). The equations of motion and the combined controller are all implemented in the Matlab/Simulink software environment. The ride efficiency of SHCIs with a Fuzzy –PID controller evaluated and compared with passive cab hydraulic isolation system (PHCIs) of original wheel loader under different movement conditions.

2 Mathematical model of earth-moving machinery

A structural diagram of a wheel loader representing the earth-moving machinery is selected as the research object, as shown in Figure1 which consists of front and rear vehicle body, cab body and driver seat masses, the front and rear vehicle body connect with the ground surface through front and rear tires, cab body connects with rear vehicle body through cab isolation system, driver seat connects with the floor of the cab through suspension system. A vehicle - road coupled interaction model of a wheel loader is set up on the basis of the structural diagram of Fig. 1, as shown in Fig. 2 where, m_{b1} is the masses of the bucket, front axle, front frame and other parts above the front wheel, m_{b2} and I_{b2} are the masses and mass inertia moments of the engine, powertrain, rear axle and other parts above the rear wheel, respectively, m_c and I_c are the mass and mass inertia moment of cab body, k_{ti} are the stiffness coefficient of the tires, c_{ti} are the damping coefficient of the tires, k_s is the stiffness coefficient of driver seat suspension system, c_s is the damping coefficient of driver seat suspension system, F_{ci} are the vertical forces of cab isolation system, l_j are the calculated distances for determining the coordinates, q_{ti} are the ground surface excitations, F_t and M_t are the replacement force and moment for the front vehicle body mass assembly, respectively, two structural diagrams of passive cab hydraulic isolation (PHCIs) and semi-active hydraulic cab isolation (SHCI), (i=1÷2, j=1÷9).

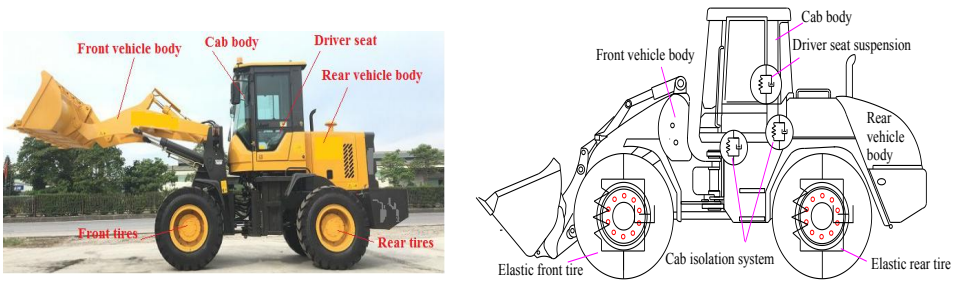

Fig. 1. Structural diagram of a wheel loader

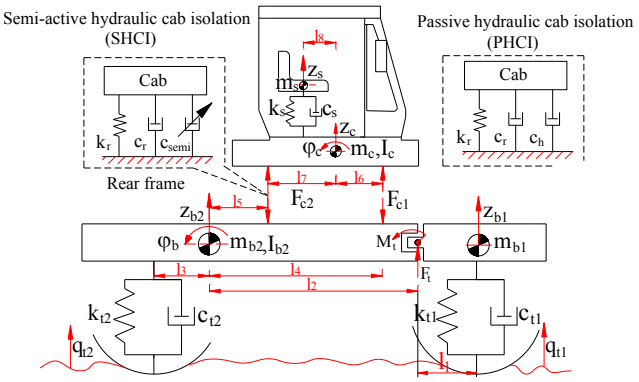

Fig. 2. A vehicle - road coupled interaction model of a wheel loader

Based on vehicle - road coupled interaction model of a wheel loader in Fig. 2, the motion equations of m_{b2}, m_c and m_s are written by Newton's law using as follows
The motion equations of m_b are written as follows

$$m_{b2}\ddot{z}_{b2} = \sum_{i=1}^{2} F_{ci} - F_{t2} + F_t \tag{1}$$

$$I_{b2}\ddot{\varphi}_{b2} = F_{t2}.l_3 - F_t l_2 + \sum_{i=1}^{i=2} F_{ci} l_{i+3} - M_t \tag{2}$$

The motion equations of m_c are written as follows

$$m_c \ddot{z}_c = F_s - \sum_{i=1}^{2} F_{ci} \tag{3}$$

$$I_c \ddot{\varphi}_c = \sum_{i=1}^{i=2} (-1)^{i+1} F_{ci} l_{i+5} - F_s l_8 \tag{4}$$

The motion equation of m_s are written as follows

$$m_s \ddot{z}_s = -F_s \tag{5}$$

where, F_t is the vertical force acting on m_{b1} which is determined by Eq. (6), F_{t2} is the vertical force acting on m_{b2} which is determined by Eq.(7), F_{ci} are the vertical forces acting on m_c which are determined by Eq.(8) and Eq.(9), M_t is the replacement moment for the front vehicle body mass assembly which is determined by Eq.(10).

$$F_t = k_{t1}\left(z_{b1} - q_{t1}\right) + c_{t1}\left(\dot{z}_{b2} - \dot{q}_{t1}\right) \tag{6}$$

$$F_{t2} = k_{t2}\left(z_{b2} - \varphi_{b2} l_4 - q_{t2}\right) + c_{t2}\left(\dot{z}_{b2} - \dot{\varphi}_{b2} l_4 - \dot{q}_{t2}\right) \tag{7}$$

$$F_{c1} = \begin{cases} k_r\left(z_c + \varphi_c l_6 - z_{b2} - \varphi_{b2} l_4\right) + c_r\left(\dot{z}_c + \dot{\varphi}_c l_6 - \dot{z}_{b2} - \dot{\varphi}_{b2} l_4\right) \\ + c_h\left|\dot{z}_c + \dot{\varphi}_c l_6 - \dot{z}_{b2} - \dot{\varphi}_{b2} l_4\right|\left(\dot{z}_c + \dot{\varphi}_c l_6 - \dot{z}_{b2} - \dot{\varphi}_{b2} l_4\right) & with \quad PHCIs \\ k_r\left(z_c + \varphi_c l_6 - z_{b2} - \varphi_{b2} l_4\right) + c_r\left(\dot{z}_c + \dot{\varphi}_c l_6 - \dot{z}_{b2} - \dot{\varphi}_{b2} l_4\right) & with \quad SHCIs \\ + c_{semi}\left|\dot{z}_c + \dot{\varphi}_c l_6 - \dot{z}_{b2} - \dot{\varphi}_{b2} l_4\right|\left(\dot{z}_c + \dot{\varphi}_c l_6 - \dot{z}_{b2} - \dot{\varphi}_{b2} l_4\right) \end{cases} \tag{8}$$

$$F_{c2} = \begin{cases} k_r\left(z_c - \varphi_c l_7 - z_{b2} - \varphi_{b2} l_5\right) + c_r\left(\dot{z}_c - \dot{\varphi}_c l_7 - \dot{z}_{b2} - \dot{\varphi}_{b2} l_5\right) \\ + c_h\left|\dot{z}_c - \dot{\varphi}_c l_7 - \dot{z}_{b2} - \dot{\varphi}_{b2} l_5\right|\left(\dot{z}_c - \dot{\varphi}_c l_7 - \dot{z}_{b2} - \dot{\varphi}_{b2} l_5\right) & with \quad PHCIs \\ k_r\left(z_c - \varphi_c l_7 - z_{b2} - \varphi_{b2} l_5\right) + c_r\left(\dot{z}_c + \dot{\varphi}_c l_7 - \dot{z}_{b2} - \dot{\varphi}_{b2} l_5\right) & with \quad SHCIs \\ + c_{semi}\left|\dot{z}_c - \dot{\varphi}_c l_7 - \dot{z}_{b2} - \dot{\varphi}_{b2} l_5\right|\left(\dot{z}_c - \dot{\varphi}_c l_7 - \dot{z}_{b2} - \dot{\varphi}_{b2} l_5\right) \end{cases} \tag{9}$$

$$M_t = \left[k_{t1}\left(z_{b1} - q_{t1}\right) + c_{t1}\left(\dot{z}_{b2} - \dot{q}_{t1}\right)\right] l_1 \tag{10}$$

where, k_r and c_r are the stiffness and damping coefficients of the main rubber part, c_h is damping coefficient of hydraulic actuator.

The ground surface excitations: Earth-moving machinery often moves on bad ground surface conditions (off-road conditions) such as high amplitude and low frequency of bumpy ground surface, ground deformation. The bad ground surface conditions with large bumps according to ISO 8608: 2016 [11] is selected as excitation functions for vehicle - road coupled interaction model of a wheel loader which is defined as

$$q(t) = \sum_{i=1}^{N} \sqrt{2G_d\left(n_i\right)\Delta n_i}\cos\left(2\pi i \Delta n t + \beta_i\right) \tag{11}$$

where, $G_d(n_i)$ is the power spectral density (PSD) at frequency n_i which defined from ISO class A to ISO class H according to ISO 8608: 2016, Δn_i is the variance of the road surface profile which depends on the spatial frequency and the time step, β_i is the phase of the harmonic function (rad) which is randomly generated between 0 and π.

3 Controller design for SHCI

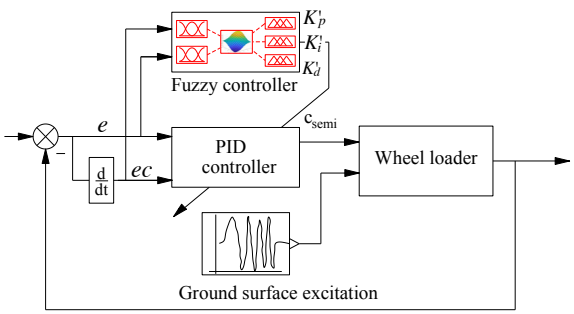

Fig. 3. Block diagram of Fuzzy –PID controler

Tuning of PID controllers using Fuzzy logic: The closed loop feedback error e=e(t) and the derivative of error ec=de(t)/dt are given as inputs to the fuzzy logic controller and the outputs are taken as the PID parameters $K_p^{'}$, $K_i^{'}$, $K_d^{'}$. The PID controller is included in the control structure in Fig. 3. In order to provide the values $K_p^{'}$, $K_i^{'}$, $K_d^{'}$ to the PID controller based on the current condition of {e, ce}.

The design simplicity PID can be easily incorporated in both linear and nonlinear systems. The definition of PID control is as follows

$$c_{semi} = K_p e(t) + K_i \int e(t)dt + K_d \frac{d}{dt} e(t) \tag{12}$$

where, K_p, K_i and K_d are called the proportional, integral and derivative gains, respectively.

Ziegler-Nichols method is one of the good online calculation tuning methods. The variable ranges of PID controller parameters are identified as follows

$$\begin{aligned} K_p^{'} &= \frac{K_p - K_{p\min}}{K_{p\max} - K_{p\min}} = \frac{K_p - K_{p\min}}{\Delta K_p} \\ K_i^{'} &= \frac{K_i - K_{i\min}}{K_{i\max} - K_{i\min}} = \frac{K_i - K_{i\min}}{\Delta K_i} \\ K_d^{'} &= \frac{K_d - K_{d\min}}{K_{d\max} - K_{d\min}} = \frac{K_d - K_{d\min}}{\Delta K_d} \end{aligned} \tag{13}$$

Hence, we obtain as follows

$$\begin{aligned} K_p &= K_p^{'}.\Delta K_p + K_{p\min} \\ K_i &= K_i^{'}.\Delta K_i + K_{i\min} \\ K_d &= K_d^{'}.\Delta K_d + K_{d\min} \end{aligned} \tag{14}$$

Where, $K_p^{'}, K_i^{'}$ and $K_d^{'}$ are the control parameters of the Fuzzy control in the variable ranges of the PID control of $\{K_{p\min} \le K_p \le K_{p\max}\}$, $\{K_{i\min} \le K_i \le K_{i\max}\}$, and $\{K_{d\min} \le K_d \le K_{d\max}\}$. The range of each parameters are as $\{100 \le K_p \le 2100\}$, $\{10 \le K_i \le 100\}$, their values are then replaced into Eq. (14) as follows

$$\begin{aligned} K_p &= 2000K_p^{'} + 100 \\ K_i &= 99K_i^{'} + 10 \\ K_d &= 9.9K_d^{'} + 0.1 \end{aligned} \tag{15}$$

By replacing Eq. (15) into Eq. (12), the PID's transfer function is achieved by

$$c_{ctr} = \left(2000K_p^{'} + 100\right)e(t) + \left(99K_i^{'} + 10\right)\int e(t)dt + \left(9.9K_d^{'} + 0.1\right)\frac{d}{dt}e(t) \tag{16}$$

The Fuzzy controller is fed with two inputs error (e) and derivative of error (ec) and the fuzzy controller output is used to adjust the PID parameters. Fuzzy inference block of the controller design is shown in Fig. 4.

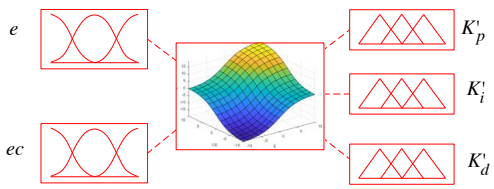

Fig. 4. Fuzzy inference block

Table 1. Control rules of Fuzzy- PID control [14]

$\{K_p^{'}, K_i^{'}, K_d^{'}\}$		ce						
		NB	NM	NS	ZE	PS	PM	PB
e	NB	NB	NB	NB	NB	NM	NS	ZE
	NM	NB	NB	NB	NM	NS	ZE	PS
	NS	NB	NB	NM	NS	ZE	PS	PM
	ZE	NB	NM	NS	ZE	PS	PM	PB
	PS	NM	NS	ZE	PS	PM	PB	PB
	PM	NS	ZE	PS	PM	PB	PB	PB
	PB	ZE	PS	PM	PB	PB	PB	PB

The membership functions for both error e and ec are taken as {Negative Big (NB), Negative Medium (NM), Negative Small (NS), Zero (ZE), Positive Small (PS), Positive Medium (PM), Positive Big (PB)}. There are 49 rules in the rule base, as shown in Table 1.

4 Results and Discussion

The equations of motion of the vehicle dynamics system in Fig. 2 and Fuzzy-PID controller are implemented in software MATLAB / Simulink with vehicle and PHCI parameters of the reference [21]. The comparison results of the vertical drive seat acceleration (a_s) and cab angular acceleration (a_{phi}) with SHCIs and PHCIs when vehicle on the poor ground surface condition (ISO class D) at v=15 km/h and empty load are shown in Figure 5. The comparison results of Fig. 5 show that the peak amplitude values of a_s and a_{cphi} with SHCIs respectively decrease compared to PHCIs that leads to a significant improvement in ride comfort of wheel loader.

Similarly, the comparison results of PSD a_s and PDS a_{phi} with SHCIs and PHCIs when vehicle on the poor ground surface condition (ISO class D) at v=15 km/h and empty load are shown in Fig. 6. The comparison results are obtained in the frequency domain in Figure 6, we show that the peak amplitude values of PSD a_s and PDS a_{phi} with SHCIs respectively significantly reduce compared to PHCIs which indicates that the efficiency of the combined controller has greatly improved the ride comfort of vehicle under large amplitude and low frequency excitations of ground surface. Especially, the peak amplitude values of PSD a_s with SHCIs respectively reduce by 38.63 %, 28.09% and 73.69 % compared to PHCIs at low frequencies as 3.40 Hz, 3.699 Hz and 6.099 Hz and the peak amplitude values of PSD a_{cphi} with SHCIs respectively reduce by 47.93 % and 82.34 % compared to PHCIs at low frequencies as 2.033 Hz and about 4.766 Hz. The ride efficiency of SHCIs has significantly reduced the resonance amplitudes of the dynamic system of vehicle compared to PHCIs at low frequencies that are sensitive to human body.

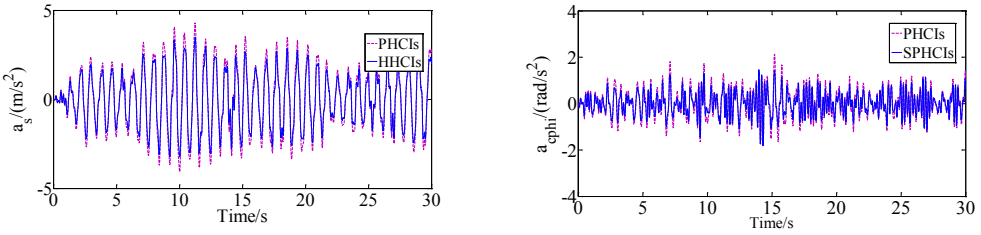

(a) Vertical driver seat *(b) Pitching angle of cab*

Fig. 5. Results comparing the acceleration responses with SHCIs and PHCIs

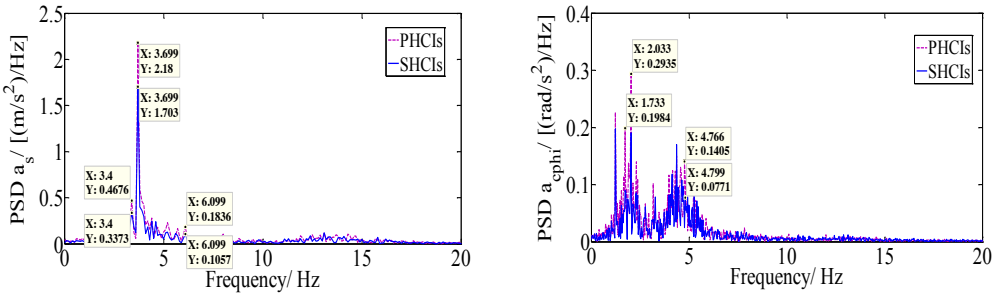

(a) Vertical driver seat *(b) Pitching angle of cab*

Fig. 6. Results comparing the PSD acceleration responses with SHCIs and PHCIs

Table 2. The values of a_{ws} and a_{wcphi} with the changing vehicle speed conditions

Parameters	v=5 km/h		v=10 km/h		v=15 km/h		v=20 km/h	
	a_{ws} (m/s^2)	a_{wcphi} (rad/s^2)	a_{ws} (m/s^2)	a_{wcphi} (rad/s^2)	a_{ws} (m/s^2)	a_{wcphi} (rad/s^2)	a_{ws} (m/s^2)	a_{wcphi} (rad/s^2)
PHCIs	1.0467	0.4436	1.4667	0.5161	1.8496	0.6235	1.9489	0.7113
SHCIs	0.8651	0.3641	1.1811	0.4188	1.5161	0.5077	1.6218	0.5834
Reduction	20.99%	21, 83%	24.18 %	23.23 %	21.33 %	22.81 %	20.17 %	21.92 %

The ride effectiveness of SHCIs in comparison with PHCIs is further verified under vehicle movement conditions, the values of a_{ws} and a_{wcphi} are defined based on ISO 2631 (1997) [12] when vehicle moves on the poor ground surface condition (ISO class D) at the condition of vehicle speed change and empty vehicle load, as shown is Table 2. From the results of Table 2, we show that the values of a_{ws} and a_{wcphi} with SHCIs respectively decrease compared to PHCIs that leads to a significant improvement in ride comfort of wheel loader when vehicle speed value increases.
The values of a_{ws} and a_{wcphi} when vehicle moves on the changing ground surface conditions at v=15 km/h and empty vehicle load are shown is Table 3. From the results of Table 3, we show that the values of a_{ws} and a_{wcphi} with SHCIs respectively decrease compared to PHCIs that leads to a significant improvement in ride comfort of wheel loader when the ground condition becomes bad.

Table 3. The values of a_{ws} and a_{wcphi} with the changing ground surface conditions

Parameters	ISO class C		ISO class D		ISO Class E	
	a_{ws}/ (m/s^2)	a_{wcphi}/(rad/s^2)	a_{ws}/(m/s^2)	a_{wcphi}/(rad/s^2)	a_{ws}/(m/s^2)	a_{wcphi}/(rad/s^2)
PHCIs	1.0583	0.3751	1.8496	0.6235	3.2626	1.0876
SHCIs	0.8944	0.3005	1.5161	0.5077	2.6597	0.9572
Reduction	18.33%	24, 83%	21.33 %	22.81 %	13.62 %	22.67 %

5 Conclusions

In this paper, a vehicle - road coupled interaction model of a wheel loader is set up under the random excitation of ground surface and a Fuzzy –PID controller is designed for control of the damping coefficient of (SHCIs). The equations of motion and the combined controller are all implemented in the Matlab/Simulink software environment. The obtained results have shown that the peak amplitude values of a_s and a_{cphi} with SHCIs respectively decrease compared to PHCIs that leads to a significant improvement in ride comfort of wheel loader and the peak amplitude values of PSD a_s and a_{cphi} with SHCIs respectively reduce by 38.63 %, 28.09%, 73.69 % and 47.93 %, 82.34 % compared to PHCIs at low frequency excitations of ground surface. Finally, the ride effectiveness of SHCIs in comparison with PHCIs was verified under vehicle movement conditions and the verified results have shown that SHCIs with PID-Fuzzy control is remarkably improved vehicle ride comfort under large amplitude and low frequency excitations of ground surface.

Acknowledgment

The work described in this paper was supported by Thai Nguyen University (TNU), Thai Nguyen University of Technology (TNUT) for a scientific project (Code: DH2019 –TN02 - 01).

References

1. R.P. Blood, P.W. Rynell, P.W. Johnson, *Journal of Safety Research* **43,** 5-6 (2012)
2. X. Zhao, K. Michael, S. Christian, *Vehicle System Dynamics* **51**, 10 (2013)
3. X. Zhao, C. Schindler, *International Journal of Industrial Ergonomics* **44**, 6 (2014)
4. F. Chi, J. Zhou, Q. Zhang, Y. Wang, P. Huang, *International Journal of Environmental Research and Public Health* **14**, 3 (2017)
5. Z. Wang *Applied Mechanics and Materials* **121-126** (2011)
6. N. Pavlov, E. Sokolov, M. Dodov, S. Stoyanov, *MATEC Web of Conferences* **133** (2017)
7. A. Rehnberg, L. Drugge, *International Journal of Vehicle Systems Modelling and Testing* **3**, 3 (2008)
8. X. Li, W. Lv, W. Zhang, H. Zhao *Journal of Vibroengineering* (2017)
9. Sh. Wang, Z. Lu, X. Liu, Y. Cao, X. Li *International Journal of Advanced* (2018)
10. T. Wei, L. Zhiqiang, *Shock and Vibration* (2019)
11. ISO 8068, *Mechanical Vibration-Road Surface Profiles – Reporting of Measured Data* (2016)
12. ISO 2631-1, *Mechanical Vibration and Shock-Evaluation of Human Exposure to Whole Body Vibration-Part 1: General Requirements* (1997)
13. X. Sun, J. Zhang *J. Vibr. Contr.* **20** (2012)
14. V. Nguyen, J. Zhang et al., *Shock Vibr.* (2018)
15. Q.V. Le, K.T. Nguyen *App. Mech. Mater.* **875** (2018)
16. L.V. Quynh, J.R. Zhang et al., *Adv. Mater. Res.* **199-200** (2011)
17. L.V. Quynh, V.T.P. Thao, T.T. Phong, *Vibroeng. Procedia* **31** (2020)
18. L.V. Quynh, N.T. Duy, N. Van Liem, B. Van Cuong, *Advances in Engineering Research and Application* (2020)
19. V. Nguyen, R. Jiao et al., *Math. Mod. Eng.* **5** (2019)
20. V. Le, J. Zhang et al., *Vibroengineering Procedia* **31** (2020)
21. L.V. Quynh, Dynamic analysis and control of cab mount system for construction machine, Science research topic: Thai Nguyen University, Thai Nguyen, Vietnam (2021)